Hindawi
International Journal of Chemical Engineering
Volume 2019, Article ID 3693657, 11 pages
https://doi.org/10.1155/2019/3693657

Research Article

Pressure Drop in Plate Heat Exchangers for Single-Phase Convection in Turbulent Flow Regime: Experiment and Theory

Sergej Gusew and René Stuke

FUNKE Wärmeaustauscher Apparatebau GmbH, Department Research and Development, Zur Dessel 1, 31028 Gronau (Leine), Germany

Correspondence should be addressed to René Stuke; stuke@funke.de

Received 20 November 2018; Revised 13 February 2019; Accepted 24 February 2019; Published 9 April 2019

Academic Editor: Junwu Wang

Plate heat exchangers (PHEs) play an important role in different technical fields, namely, in energetics, chemical industry, food industry, and others. To use PHE effectively, it is necessary to have correct data for pressure drop. Unfortunately, in open literature, a large difference among different authors occurs. In this work is shown that an essential portion of this difference lies in the choice of the typical length for the calculation of the friction coefficient. Care must be taken to consider the pressure drop of the distribution zone. A three-component model for hydraulic resistance of PHE in turbulent flow regime is proposed in this work. The proposed model shows good agreement with experimental data.

1. State of Research

Plate heat exchangers (PHE) are widely used in industry. A compact size due to high heat transfer coefficients is one major advantage over other heat exchanger types like shell and tube type. The special design of the flow channels results in early transition from laminar to turbulent flow and significant increase in heat transfer coefficients. Unfortunately, this comes along with an increase in pressure drop compared to flat channels, too. A reliable model for pressure drop calculation is required for a successful use of PHE.

The following model is traditionally applied to present experimental data of a PHE:

$$\Delta p = 4 f_{\mathrm{ch}} \cdot \frac{\rho w^2}{2} \cdot \frac{L}{D_{\mathrm{e}}}, \tag{1}$$

where Δp is the pressure drop in a channel of a PHE, w is the average velocity in a channel, L is the effective length of the PHE, D_{e} is the equivalent diameter of a channel, and f_{ch} is the Fanning friction factor or Fanning factor in a channel.

In literature, the model according to equation (1) is widespread [1–19]. The Fanning friction factor is a function of Reynolds number and is presented in graphical or analytical form. If Fanning factors were found for a specific unit, this model can reproduce the specific unit's pressure drop within 10% to 20% margin. Applied to a PHE with different geometries, the margin of deviation can be much higher. Fanning factors calculated with models of different authors can vary by up to 50–100%. Therefore, Fanning factors found for one plate type are mostly valid only for its specific design. Applications of equation (1) to various PHEs are stated in textbooks of Wang et al. [20] and Klemes et al. [21]. Some results cannot be explained well according to equation (1). The study [2] is a good example: it shows different correlations for refrigerants R 245fa and R 236a in turbulent flow regime for the same PHE. This means that equation (1) cannot always consider a strong influence of physical properties correctly.

Two citations of recent publications summarize the state of the art very well:

(i) "Most of the previously reported empirical correlations are restricted to specific experimental geometry and flow conditions and cannot be generalized for all PHE applications" [9].

(ii) "It can be seen from the experimental studies. . ., a general correlation applicable to all chevron angle even with the same chevron angle is not possible. A gasketed plate heat exchanger design continues to be proprietary in nature; the correlations obtained are applicable to this exchanger that is marketed" [12].

Several attempts of creating a generalized theory were made in the past. Especially, Dovic et al. [7], Martin [14], Muley and Manglik [16], Klemes et al. [21], and Arsenyeva et al. [22] deserve attention. The most physically reasonable approach is the three-component model proposed by Arsenyeva et al. [23].

This work is dedicated to study the influence of reference length L on the pressure drop of a PHE. At first, it is shown that usage of the model according to equation (1) results in Fanning factors that always depend on effective length L. Subsequently, the three-component model proposed by Arsenyeva et al. [23] is enhanced. It divides the channel in the two distribution zones—at the inlet and outlet of a channel—and the corrugation field in the middle of a channel. Each of the three zones of the channel has its own friction factor correlation. Furthermore, it is shown that the corrugation field correlation has universal characteristics and is independent of its length in turbulent regime.

2. Experimental Setup and Procedure

Experimental setup involves three PHEs (warm-side setup, test set, and cold-side set-up), arranged in two closed loops, as shown in Figure 1.

On the warm side, a pump circulates the warm fluid (water or ISO VG46 Oil). The warm fluid is heated by using a boiler. On the cold side, three air coolers maintain a constant temperature of the fluid (water or glycol). A fully automatic control unit adjusts the temperature and flow rates to comply with the set values. As test PHE were used four plate heat exchangers of *FUNKE Wärmeaustauscher Apparatebau GmbH* (Germany) [24]. One of these plates is shown in Figure 2.

The geometric parameters of a plate are illustrated in Figure 3, and the geometric values for plates P1–P4 are shown in Table 1.

Every device could have one of the three chevron patterns: HH (with chevron angle $\varphi = 63^\circ$), HL (with chevron angle $\varphi = 63^\circ/27^\circ$), and LL (with chevron angle $\varphi = 27^\circ$).

All four plates are similar, and only the length of the corrugated field varies. In Figure 4, the test set with test PHE is shown.

Platinum resistance thermometers Pt1000 (T1–T4) are used to measure the fluid temperatures at the inlet/outlet of the test PHE with the measurement error $\pm(0.15\,\mathrm{K} + 0.002\,\mathrm{t})$. To improve the precision of the sensors, we calibrate all temperature sensors simultaneously at the area of working temperature. The deviation of measured temperature of all sensors is about 0.05–0.1 K. The flow rates in the test section are measured by volumetric inductive flow meters of type *KROHNE OPTIFLUX 4300* (MF1 and MF2) with a measurement error of ±1% for measuring range 3–500 $\mathrm{m^3/h}$. Static mixers are used to reduce local temperature variations. Static mixers (2 and 4) at outlets are basically used, mixers (1 and 3) at inlets if necessary. The pressure losses of the fluid flowing through the test section is measured with a differential pressure transmitter model DPT10 (PD1 and PD2) with the measurement error of ±0.2%. The two devices are used for measuring ranges 0–500 mbar and 0–3 bar. Pressure at the inlet of PHE is measured with the pressure transmitter (P1 and P2) with the measurement error of ±0.2%.

The values are measured as close as possible to the test PHE, taking care to use calibrated measurement pipes (length/diameter ≥ 10). The test PHE was configurated as a single-pass U-type counterflow device. The corrugation profile of the plate is given in Figure 5. It is close to sinusoidal.

All data were obtained under steady-state conditions with close energy balance (less than ±5% difference between the measured performance of warm and cold side). A constant inlet temperature (≈60°C) for the hot fluid was maintained throughout each set of experiments. The inlet temperature of the cold fluid was constant (≈40°C), too. All sensors and measuring equipment are calibrated accordingly to standard ISO 9001 : 2008.

3. Data Reduction

The primary measurements of each fluid consist of the flow rate, inlet and outlet temperatures, pressure drop between the inlet and outlet of the PHE, and inlet pressure for every side. The channel flow Reynolds number is based on the equivalent diameter D_e:

$$D_e = 2t. \tag{2}$$

All fluid properties were calculated at the bulk-mean temperature given by

$$T_{mean} = 0,5\left(T_{inlet} + T_{outlet}\right). \tag{3}$$

From the measured overall pressure drop across the PHE Δp_{measur}, the pressure drop in the channel can be obtained from the following equation:

$$\Delta p_{ch} = \Delta p_{measur} - \Delta p_{port} - \Delta p_{pipe}. \tag{4}$$

For the port, pressure drop according to [17] is used:

$$\Delta p_{port} = 1.5 \cdot \frac{\rho w_{port}^2}{2}. \tag{5}$$

The pressure loss in inlet and outlet pipe Δp_{pipe} was estimated on the basis of the smooth tube friction factor, and local pressure losses on the sudden area changes. The pressure loss Δp_{pipe} considers the distance of pressure sensors to PHE.

The Fanning friction factor was calculated as

$$f_{ch} = \frac{\Delta p_{ch}}{2\rho w_{ch}^2 \cdot L/D_e}. \tag{6}$$

The choice of effective length of the PHE L is discussed later.

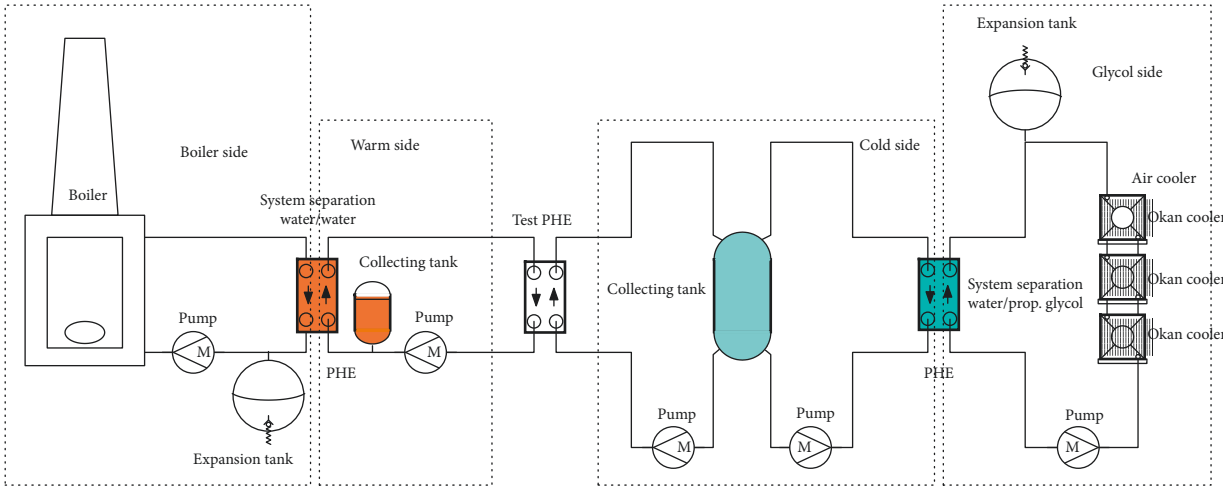

Figure 1: Experimental setup.

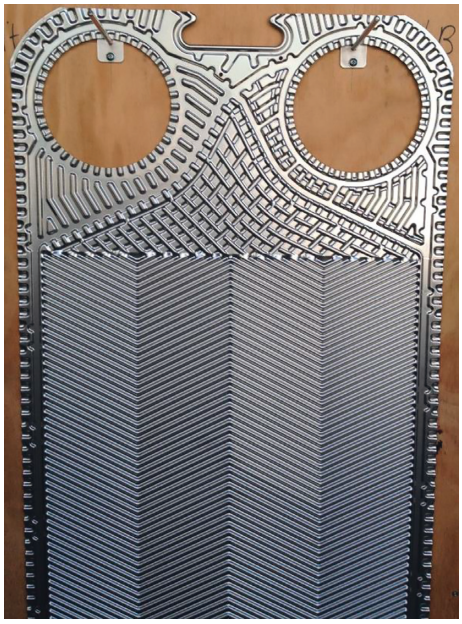

Figure 2: Experimental plate P2.

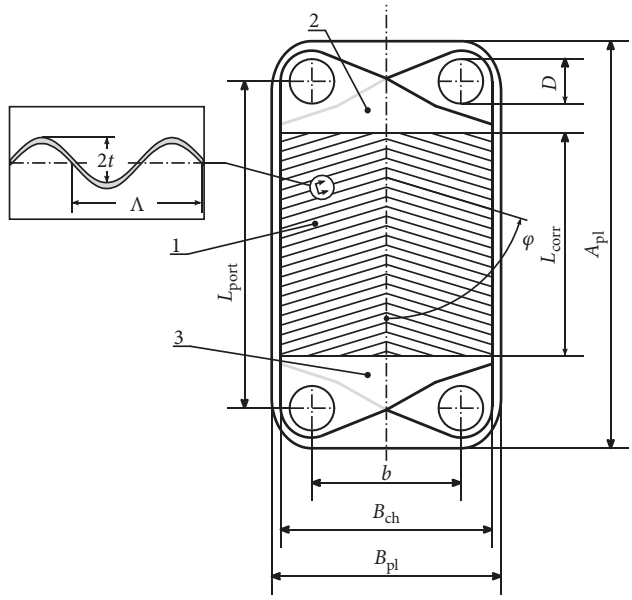

Figure 3: Geometrical parameters of a plate. (1) Corrugated field, (2) inlet distribution zone, and (3) outlet distribution zone.

The experimental uncertainties were determined by the procedure outlined by [25]. The maximum errors in the primary measurements of flow rate $\dot{M}$, pressure drop Δp, and temperature T were ±1%, ±0.2%, and ±(0.15 K + 0.002 T), respectively. Based on these measurement uncertainties and the propagation of error analysis, the uncertainties in Reynolds number Re and Fanning friction factor f were 5.7% and 9.2%, respectively.

4. Experimental Results

For the valid presentation of the data for the pressure losses in the channel of PHEs, the choice of the characteristic length L of the PHEs is important. In common use is the vertical distance between holes in the plate L_{port} [14, 16]:

$$L = L_{port}. \tag{7}$$

Some authors use the relation between the area of the plate and its width [3, 5]:

$$L = \frac{A_{proj} \cdot FK}{B_{ch}}. \tag{8}$$

The authors [10] consider the choice:

$$L = L_{port} - D. \tag{9}$$

For comparison, all our data and data of other authors have been processed with a characteristic length according to equation (7). Results for plate P2 are presented in Figure 6. For each chevron pattern, three zones can be identified graphically [16]:

(1) Laminar zone without vortices, Re < 100

(2) Vortices zone, 100 < Re < 500

Table 1: Chevron plate characteristics.

Plate	P1	P2	P3	P4
$D_e = 2t$ (mm)		5.2		
D (mm)		148		
A (m^2)	0.3634	0.5618	0.7602	1.0243
L_{corr} (m)	0.592	0.957	1.322	1.808
L_{port} (m)	0.941	1.306	1.671	2.158
B_{ch} (m)		0.456		
Λ (mm)		9.0		
Δ_{wall} (mm)		0.5		
λ_{wall} (W/mK)		15		
FK		1.192		
Number of plates	19, 35, 51	17, 35, 51	51	17, 51

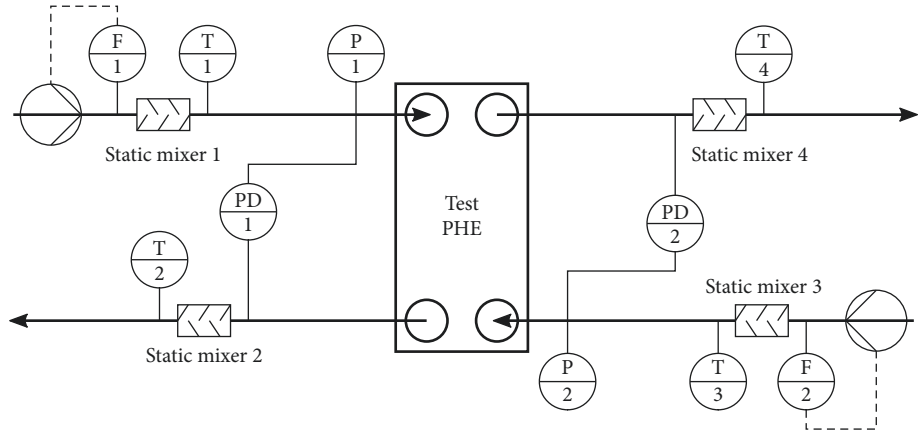

Figure 4: Test setup.

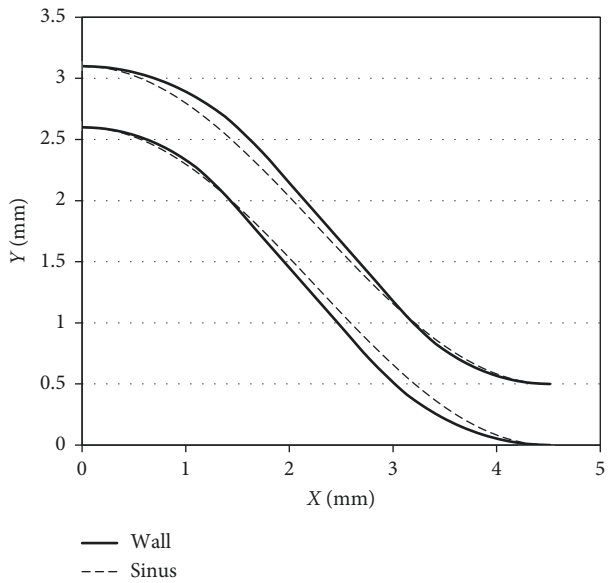

Figure 5: Corrugation profile of a plate.

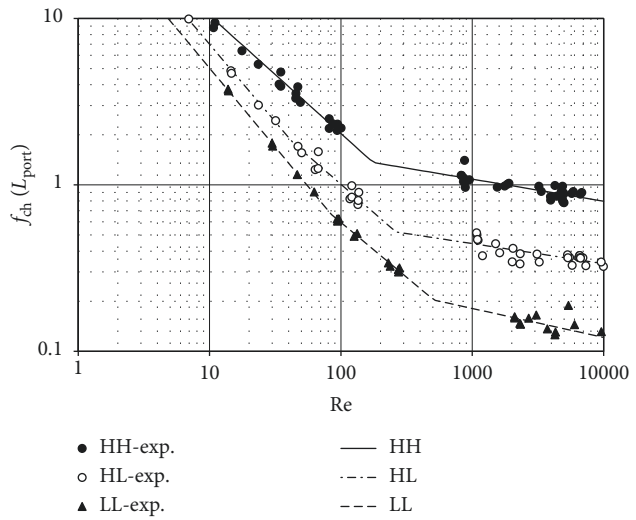

Figure 6: Fanning factor for plate P2 with 3 corrugations HH, HL, and LL.

(3) Turbulent zone, Re > 200–500

By increase in chevron angle φ, the hydraulic resistance in the channel increases and transition to turbulence is displaced to smaller Reynolds numbers.

Figure 7 illustrates experimental data in the turbulent zone for all four PHE P1–P4 with chevron pattern HH and data of other authors.

In the turbulent zone, it is obvious that data depend on plate length L_{port}: the higher the length is, the higher the Fanning friction factor is. The shortest plate P1 has the

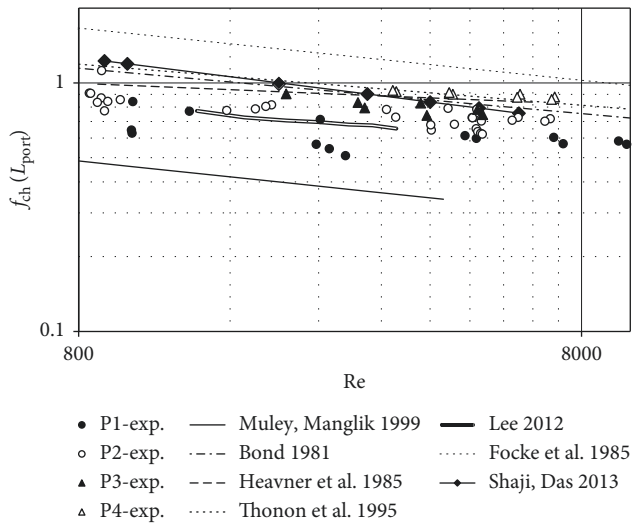

Figure 7: Fanning factor for plates P1–P4 with chevron pattern HH.

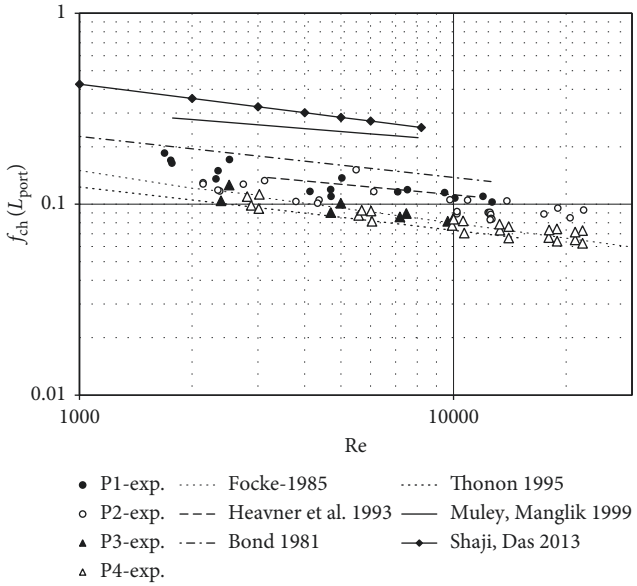

Figure 8: Fanning factor for plates P1–P4 with chevron pattern LL.

smallest friction factor. The dependence of friction factor $f_{ch}(L_{port})$ on the relative length of a plate L_{port}/B_{ch} is confirmed by comparison of our experimental data with literature, too. Our data for the long plates P3 ($L_{port}/B_{ch} = 3.69$) and P4 ($L_{port}/B_{ch} = 4.73$) agree well with the data of Bond [4], Heavner [12], and Thonon [19], who investigated industrial PHEs. Data for our shorter plates P1 ($L_{port}/B_{ch} = 2.06$) and P2 ($L_{port}/B_{ch} = 2.86$) are considerably lower.

The same characteristic behavior can be observed for data of other authors. Fanning factor f is the highest in the publication of Focke et al. [9] who used a plate with $L_{port}/B_{ch} = 4.0$. Data for a plate with $L_{port}/B_{ch} = 3.57$ from Shaji and Das [18] are lower and agree well with our data for plate P3 ($L_{port}/B_{ch} = 3.69$). Fanning factors of Lee et al. [13] for a plate with $L_{port}/B_{ch} = 2.94$ are approximately the same as our data of plate P2 ($L_{port}/B = 2.86$). Muley and Maglik [16] investigated a plate with $L_{port}/B_{ch} = 2.4$ and received considerably lower Fanning factors compared to all other mentioned authors.

In Figure 8, experimental data for plates P1–P4 with chevron pattern LL are compared to data of other authors. For corrugation angle $\varphi = 27^{\circ}$ (LL), the dependence $f_{ch}(L_{port})$ on the length L_{port} changes in comparison with HH. For LL chevron pattern, Fanning factors decrease by increase in length L_{port}. Therefore, in Figure 8, the values $f_{ch}(L_{port})$ of the shortest plate P1 are the biggest ones and values $f_{ch}(L_{port})$ for longest plate P4 are the smallest ones.

As before, our experimental data are consistent with the data of Bond [4], Heavner [12], and Thonon [19]. Generally, variation between the correlations has increased. A relatively high influence of distribution zone on channel pressure drop for LL pattern seems to be a probable cause of this behavior.

Data of Focke et al. [9] ($L/B = 4.0$) are now in the range of the lowest data. Fanning factors of Shaji and Das [18] for a plate with $L_{port}/B_{ch} = 2.4$ are the second highest now. The proportionality of the Fanning factor and plate length is not as expected for data of Shaji and Das [18]. This may be caused by different geometries of the distribution zones.

5. Three-Component Model

The typical approach (equation (6)) to make a connection between hydraulic resistance and characteristic length of the plate leads to length-dependent Fanning friction factors. The resulting correlations are of opposite behavior for low and high (LL and HH) chevron angles. It is caused by a different character of the flow in all three characteristic zones—inlet and outlet distribution zone and corrugated field. Due to this, the idea of Arsenyeva et al. [23] to divide a plate in three areas and describe the friction factor independently for each area seems reasonable.

A main challenge of a three-component model is the complexity of measurements for all components. A calculation-based approach to determine the different parts of the pressure drop is an alternative to measurements. This is possible if experimental data for one series of plates (equal corrugation type, distribution zone, and width) with different lengths of the corrugated field are available.

From experimental data, the pressure drop of a channel Δp_{ch} is received. At first, data for a low corrugation angle (LL) are used. The turbulent flow region is initially considered because of very limited amount of data in laminar region. A dimensionless form of the channel pressure drop is introduced:

$$F_{ch} = \frac{\Delta p_{ch}}{4\rho w_{ch}^2/2}. \tag{10}$$

The channel pressure drop Δp_{ch} consist of three components in this model:

$$\Delta p_{ch} = \Delta p_{corr} + \Delta p_{inlet} + \Delta p_{outlet}, \tag{11}$$

with pressure drop of the corrugated field Δp_{ch} and pressure drop of the inlet Δp_{inlet} and outlet Δp_{outlet} distribution zone. Each component is described as follows:

$$\Delta p_{\text{inlet}} = \Delta p_{\text{outlet}} = 4 f_{\text{inlet}} \cdot \frac{\rho w_{\text{ch}}^2}{2}, \tag{12}$$

$$\Delta p_{\text{corr}} = 4 f_{\text{corr}} \cdot \frac{\rho w_{\text{ch}}^2}{2} \cdot \frac{L_{\text{corr}}}{D_{\text{e}}}. \tag{13}$$

The characteristic velocity of the channel w_{ch} is used for all three zones. This makes the data handling easier, and comparability of results between distribution zones and corrugated field is improved. A main disadvantage is that velocity w_{ch} is not the physical velocity in distribution zones. The cross section in distribution zones differs from the one of the corrugated field and therefore velocity, too. As a result, friction factor f_{inlet} has only computational meaning.

From equations (10)–(13), we get

$$F_{\text{ch}} = 2 f_{\text{inlet}} + f_{\text{corr}} \frac{L_{\text{corr}}}{D_{\text{e}}}. \tag{14}$$

For PHEs P1–P4, four functions are received from experimental data:

$$F_{\text{ch}}^{i} = f_i(\text{Re}), \quad i = 1, \ldots, 4. \tag{15}$$

Characteristic values for Reynolds number in the range Re = 1000,. . ., 10000 are chosen and called Re*. Values $f_i(\text{Re}^*)$ are according to equations (14) and (15), linear depending from $L_{\text{corr}}/D_{\text{e}}$. Using known mathematical procedure, we receive linear approximation for four points $[L_{\text{corr}}/D_{\text{e}}; F_{\text{ch}}^{i}]_{i=1,\ldots,4}$ for all characteristic values of Re*. The resulting y-intercept of this linear function is $2 f_{\text{inlet}}(\text{Re}^*)$ while $f_{\text{corr}}(\text{Re}^*)$ is the slope. The obtained values are presented in Table 2.

By approximating the data from Table 2, we obtain

$$f_{\text{inlet}}(\text{Re}) = 5.525 + \frac{7500}{\text{Re}}, \tag{16}$$

$$f_{\text{corr}}(\text{Re}) = \frac{0.4305}{\text{Re}^{0.2228}}. \tag{17}$$

The deviation of equations (16) and (17) is about 5% from data of Table 2. With equation (14), dimensionless pressure drop F_{ch} becomes the form

$$F_{\text{ch}} = 11.05 + \frac{15000}{\text{Re}} + \frac{0.4305}{\text{Re}^{0.2228}} \cdot \frac{L_{\text{corr}}}{D_{\text{e}}}. \tag{18}$$

The dimensionless pressure drop can be rearranged to Fanning friction factor of the channel (equations (6) and (14)). We get

$$f_{\text{ch}} = \frac{F_{\text{ch}}}{L_{\text{corr}}/D_{\text{e}}} = \frac{2 f_{\text{inlet}}}{L_{\text{corr}}/D_{\text{e}}} + f_{\text{corr}}. \tag{19}$$

According to equation (19), Fanning factor of the channel f_{ch} is related to characteristic length L_{corr}. Earlier in Figures 6–8, the Fanning factor was based on characteristic length L_{port}. By using equations (16), (17), and (19) for plates P1–P4 with LL corrugated field, we receive

$$f_{\text{ch}} = \frac{F_{\text{ch}}}{L_{\text{corr}}/D_{\text{e}}} = \frac{11.05 + 15000/\text{Re}}{L_{\text{corr}}/D_{\text{e}}} + \frac{0.4305}{\text{Re}^{0.2228}}. \tag{20}$$

Table 2: Fanning friction factor for plates P1–P4 with LL corrugated field in turbulent flow.

Re*	f_{inlet}	f_{corr}
1000	12.47	0.09236
2000	9.74	0.08100
4000	7.59	0.07077
6000	6.56	0.06593
10000	6.40	0.05530

Calculated values from equation (20) are drawn as lines in Figure 9, and they are labeled with "Theory." As can be seen, calculated data agree well with experimental data. The deviation is within ±5%. It must be emphasized that both equations (16) and (17) are only valid for specific geometry of distribution zone and corrugated field of plates P1–P4.

Distribution zones are equal for all patterns of corrugated fields. Due to this fact, equation (16) is valid for HH and HL channels, too. Based on experimental data for pressure drop Δp_{ch} of HH and HL channels, the Fanning factor can be calculated from equations (11)–(13) for corresponding channel type.

To receive f_{corr} (HH), at first, dimensionless pressure drop is calculated for the HH corrugated field:

$$F_{\text{ch}}(\text{HH}) = \frac{\Delta p_{\text{ch}}}{4 \rho w_{\text{ch}}^2 / 2}. \tag{21}$$

This allows us to calculate the Fanning friction factor of the channel for characteristic length L_{corr}:

$$f_{\text{ch}}(\text{HH}) = \frac{F_{\text{ch}}(\text{HH})}{L_{\text{corr}}/D_{\text{e}}}. \tag{22}$$

With known $f_{\text{inlet}}(\text{Re})$ from equation (16), we get

$$f_{\text{corr}}(\text{HH}) = f_{\text{ch}}(\text{HH}) - \frac{2 f_{\text{inlet}}}{L_{\text{corr}}/D_{\text{e}}}. \tag{23}$$

Values calculated from equation (23) result in a function depending on the Reynolds number. Following approximation is obtained from experimental data of the HH channel type:

$$f_{\text{corr}}(\text{HH}) = \frac{2.809}{\text{Re}^{0.1325}}. \tag{24}$$

The Fanning factor of the channel from equations (16) and (24) is

$$f_{\text{ch}}(\text{HH}) = \frac{11.05 + 15000/\text{Re}}{L_{\text{corr}}/D_{\text{e}}} + \frac{2.809}{\text{Re}^{0.1325}}. \tag{25}$$

Calculated values of $f_{\text{ch}}(\text{HH})$ from equation (25)—labeled as "Theory"—and experimental data according to equation (22) are compared in Figure 10.

For the HH channel type, data show only a slight dependency from the length of the corrugated field. This is due to a relatively low hydraulic resistance of distribution zones compared to HH corrugated field.

All calculations according to equations (21)–(25) are performed for HL channel type, too. We get

$$f_{\text{corr}}(\text{HL}) = \frac{0.6323}{\text{Re}^{0.08736}}, \quad (26)$$

$$f_{\text{ch}}(\text{HL}) = \frac{11.05 + 15000/\text{Re}}{L_{\text{corr}}/D_{\text{e}}} + \frac{0.6323}{\text{Re}^{0.08736}}. \quad (27)$$

Calculated values of $f_{\text{ch}}(\text{HL})$ from equation (27)—labeled as "Theory"—and experimental data are compared in Figure 11.

Experimental data agree with theoretical values within ±10%, and these are compatible with the uncertainty of the measurements.

The three-component model gives the opportunity to use data sets for twelve configurations (four plate lengths with three corrugation angles each) and describes with only four correlations for friction factors: $f_{\text{inlet}}(\text{Re})$, $f_{\text{corr}}(\text{HH})$, $f_{\text{corr}}(\text{HL})$, and $f_{\text{corr}}(\text{LL})$. It is important to note that these correlations are length independent.

In Figure 12, all experimental data are compared with theoretical values for $f_{\text{corr}}(\text{Re})$ of the three-component model. For this purpose, experimental data for all channels $f_{\text{ch,exp}}$ were recalculated to experimental data for the corrugated field according to the following equation:

$$f_{\text{corr,exp}} = f_{\text{ch,exp}} - \frac{2f_{\text{inlet}}}{L_{\text{corr}}/D_{\text{e}}}. \quad (28)$$

It can be seen that data from experiments of all four plates correspond to the theoretical calculations. Experimentally is confirmed that the factor $f_{\text{corr}}(\text{Re})$ does not depend on the length of the corrugated field L_{corr}.

5.1. Dependence of Fanning Friction Factor $f_{ch}(L_{port})$ from Plate Length. Based on the proposed three-component model, a simple physical explanation of observed opposite behavior of Fanning friction factor $f_{\text{ch}}(L_{\text{port}})$ for HH and LL channels can be obtained. It is assumed that friction factor $f_{\text{inlet}}(\text{Re})$ is linear dependent from distribution zone length:

$$f_{\text{inlet}} = \text{RP}_{\text{inlet}} \frac{\left(L_{\text{port}} - L_{\text{corr}}\right)}{2D_{\text{e}}}, \quad (29)$$

where RP_{inlet} is a unique relative pressure drop coefficient for each series of plate with equal geometry of distribution zone. It describes the specific hydraulic resistance of this zone. We derive from equation (19)

$$f_{\text{ch}}\left(L_{\text{port}}\right) = \frac{F_{\text{ch}}}{L_{\text{port}}/D_{\text{e}}} = \frac{2f_{\text{inlet}} + f_{\text{corr}}L_{\text{corr}}/D_{\text{e}}}{L_{\text{port}}/D_{\text{e}}},$$

$$f_{\text{ch}}\left(L_{\text{port}}\right) = \frac{2 \cdot \text{RP}_{\text{inlet}}L_{\text{port}} - L_{\text{corr}}/2D_{\text{e}}}{L_{\text{port}}/D_{\text{e}}} + f_{\text{corr}}\frac{L_{\text{corr}}}{L_{\text{port}}}, \quad (30)$$

$$f_{\text{ch}}\left(L_{\text{port}}\right) = \text{RP}_{\text{inlet}}\frac{L_{\text{port}} - L_{\text{corr}}}{L_{\text{port}}} + f_{\text{corr}}\frac{L_{\text{corr}}}{L_{\text{port}}}.$$

We introduce the relative length of the corrugated field

$$X = \frac{L_{\text{corr}}}{L_{\text{port}}}, \quad (31)$$

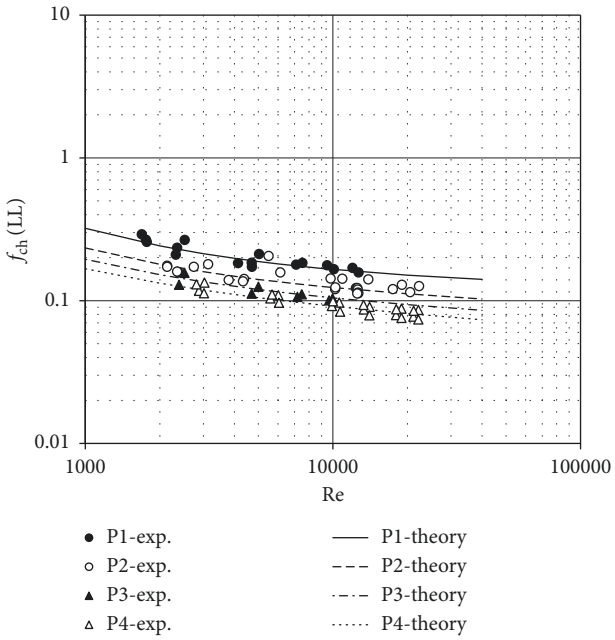

Figure 9: Fanning friction factor f_{ch} (LL) for plates P1–P4 with LL corrugated field.

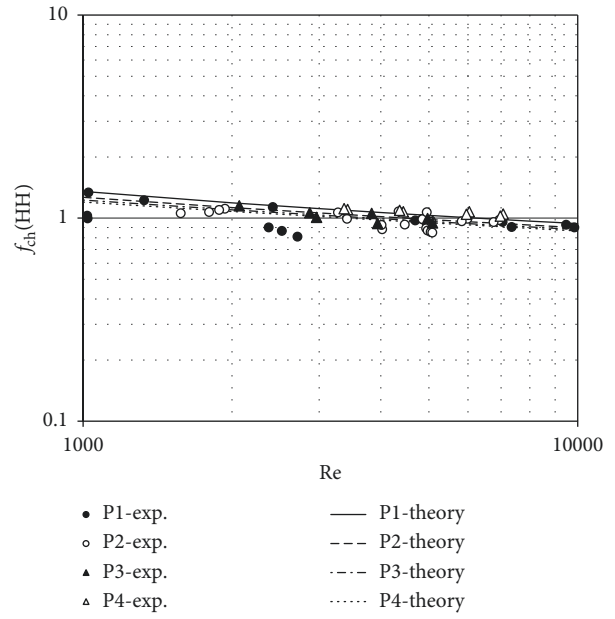

Figure 10: Fanning friction factor $f_{\text{ch}}(\text{HH})$ for plates P1–P4 with HH corrugated field.

and get

$$\begin{aligned} f_{\text{ch}}\left(L_{\text{port}}\right) &= \text{RP}_{\text{inlet}} \cdot (1 - X) + f_{\text{corr}} \cdot X \\ &= \text{RP}_{\text{inlet}} + X \cdot \left(f_{\text{corr}} - \text{RP}_{\text{inlet}}\right). \end{aligned} \quad (32)$$

By increase in plate length A_{pl}, both L_{port} and L_{corr} increase; however, length of distribution zone remains unchanged:

$$L_{\text{port}} - L_{\text{corr}} = \text{const}. \quad (33)$$

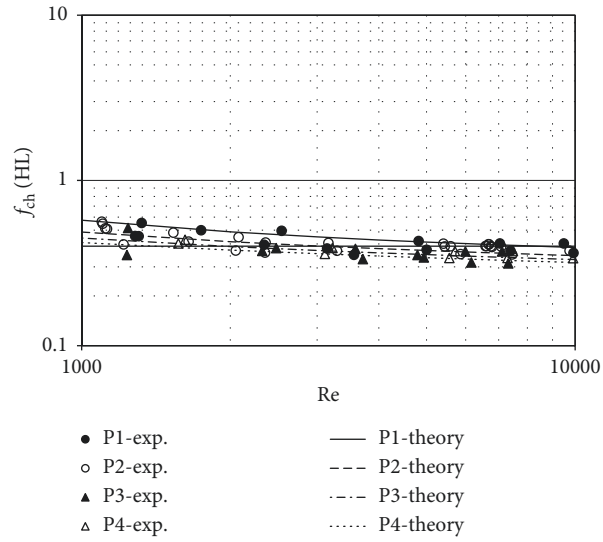

Figure 11: Fanning friction factor f_{ch} (HL) for plates P1–P4 with HL corrugated field.

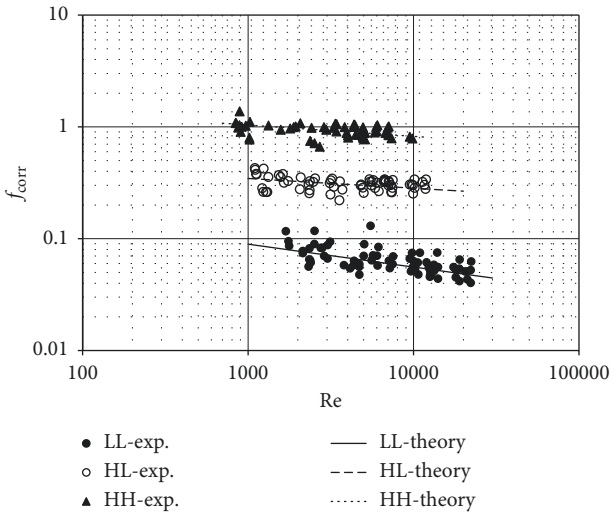

Figure 12: Fanning friction factor f_{corr} vs. Reynolds number for plates P1–P4.

With equation (31), we get,

$$1 - X = \frac{\text{const}}{L_{port}},$$
$$X = 1 - \frac{\text{const}}{L_{port}}. \tag{34}$$

As a result, if L_{port} increases, X approaches one ($X \longrightarrow 1$) and from equation (32),

$$f_{ch}\left(L_{port}\right) \longrightarrow f_{corr}. \tag{35}$$

For plates with very short corrugated field, X approaches zero ($X \longrightarrow 0$) and

$$f_{ch}\left(L_{port}\right) \longrightarrow \mathrm{RP}_{inlet} \tag{36}$$

The characteristic dependence of $f_{ch}(L_{port})$ from relative length of corrugated field X is shown in Figure 13. As a general rule, the Fanning friction factor of HH corrugated field is bigger than relative pressure drop of the inlet RP_{inlet}, while the friction factor of LL corrugated fields is smaller:

$$f_{corr}(\mathrm{HH}) > \mathrm{RP}_{inlet} > f_{corr}(\mathrm{LL}). \tag{37}$$

For example, for PHE P1–P4 at Re = 1000, the friction factor is calculated as follows:

$$\left[f_{corr}(\mathrm{HH}) = 1.125\right] > \left[\mathrm{RP}_{inlet} = 0.387\right] > \left[f_{corr}(\mathrm{LL}) = 0.09236\right]. \tag{38}$$

According to equation (35), an increase in plate length for the HH channel type should result in an increase in friction factor $f_{ch}(L_{port})$ that approaches f_{corr}(HH). LL corrugated field has a relatively low pressure drop according to equation (37); therefore, with increase in plate length, $f_{ch}(L_{port})$ should decrease and approach f_{corr}(LL). Our experimental data confirm this behavior.

5.2. Pressure Drop Fraction in Inlet and Outlet Distribution Zones. It is important to know what part of overall channel pressure drop corresponds to distribution zone. We introduce the inlet pressure drop ratio IR(Re):

$$\mathrm{IR}(\mathrm{Re}) = \frac{2\Delta p_{inlet}}{\Delta p_{ch}}. \tag{39}$$

With equations (10) and (12), IR(Re) can be written as

$$\mathrm{IR}(\mathrm{Re}) = \frac{2f_{inlet}}{f_{ch} \cdot L_{corr}/D_e} \tag{40}$$

$$\text{or } \mathrm{IR}(\mathrm{Re}) = \frac{1}{1 + f_{corr}/f_{inlet} \cdot L_{corr}/2D_e}. \tag{41}$$

Equation (41) shows that always IR(Re) < 1. The higher IR(Re) is, the higher the portion of pressure drop in distribution zones is. For plates P1–P4, Figures 14–16 show calculated values for IR(Re) for all three channel types.

The inlet pressure drop ratio IR(Re) is highest in shortest plate P1 with LL corrugation angle. It is between 66% and 77%. Plates P2–P4 show values from 39% up to 61% as it can be seen in Figure 14. Plates with HH corrugated field shows values from 12% to 17% for shortest plate P1 (Figure 16). Longer plates have an inlet pressure drop ratio IR(Re) from 4% up to 11%. The results of intermediate corrugation angle HL lay in-between HH and LL channels. Values for IR(Re) from 28%–40% for plate P1 and 11%–29% for plates P2–P4 are calculated.

The calculated values of inlet pressure drop ratio show that the distribution zones play an important role in channel pressure drop for chevron angles of 30°–45° and lower.

5.3. Comparison of the Three-Component Model to Existing Data. Our approximation for the pressure drop factor of distribution zone f_{inlet}(Re) (equation (16)) is received by investigation of plates with particular distribution zone. Arsenyeva et al. [23] show the following equation:

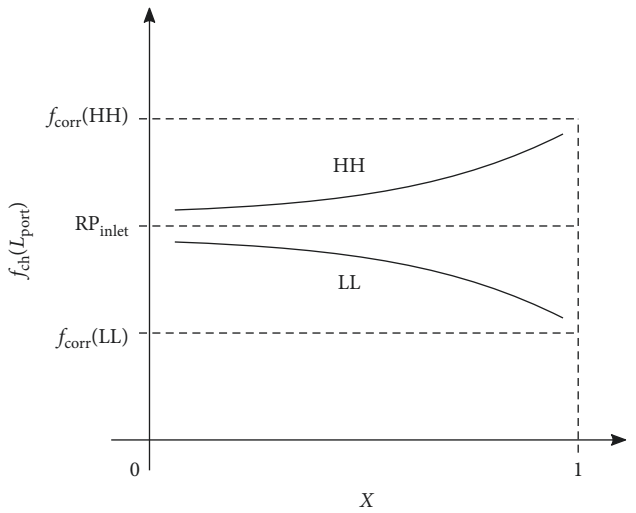

Figure 13: Characteristic dependence of friction factor $f_{ch}(L_{port})$ from relative length of corrugated field X.

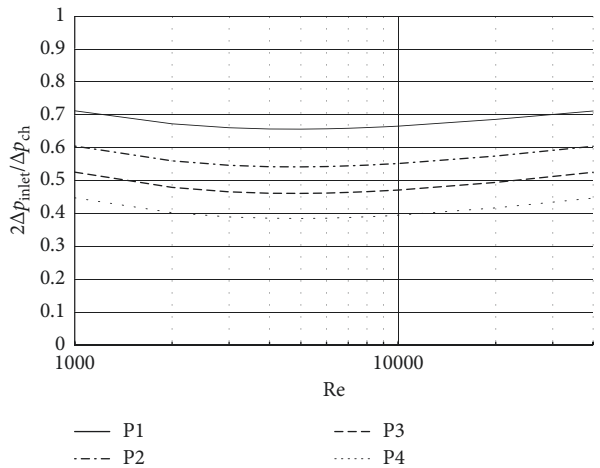

Figure 14: Inlet pressure drop ratio IR(Re) for plates P1–P4 for LL corrugated field.

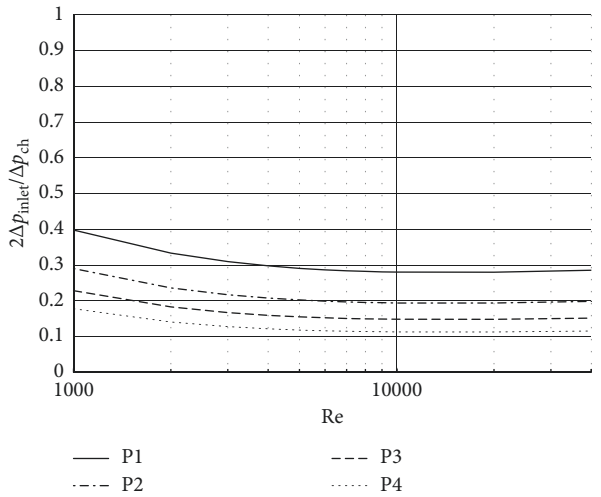

Figure 15: Inlet pressure drop ratio IR(Re) for plates P1–P4 for HL corrugated field.

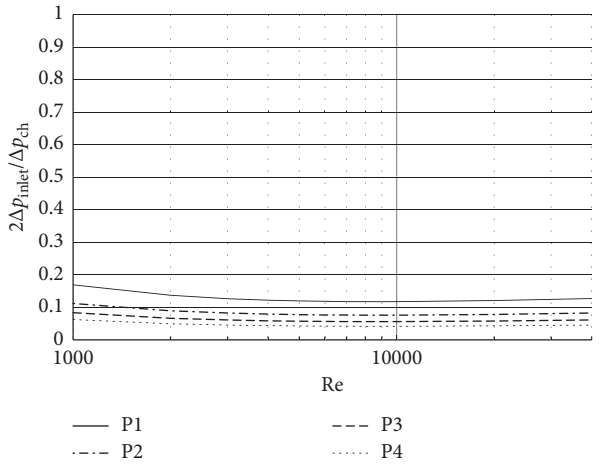

Figure 16: Inlet pressure drop ratio IR(Re) for plates P1–P4 for HH corrugated field.

$$\Delta p_{inlet} = f_{DZ} \cdot \frac{\rho w_{ch}^2}{2}, \tag{42}$$

with friction coefficient f_{DZ} calculated by

$$f_{DZ} = 38 \cdot \frac{f_{ch}(\mathrm{Re}, \varphi = 65^\circ)}{f_{ch}(\mathrm{Re} = 2700, \varphi = 65^\circ)}. \tag{43}$$

This equation is also obtained for a particular plate design. Therefore, a full quantitative match with our data can not be expected. Nevertheless, a comparison is of interest.

By comparing equations (12) and (42), it has to be noted that

$$f_{inlet}(\mathrm{Re}) = \frac{f_{DZ}(\mathrm{Re})}{4}. \tag{44}$$

For Re = 2700, we get from equation (43), $f_{DZ} = 38$ and according to equation (44), $f_{inlet} = 38/4 = 9.5$ and from equation (16), $f_{inlet} = 5.525 + 7500/2700 = 8.3$.

The difference between equations (43) and (16) is about 13%; this is within the range of experimental uncertainties. Figure 17 shows calculated values of equations (43), (44), and (16). In the range Re = 1000, . . ., 40000, values from both equations agree well.

6. Conclusions

(i) Pilot study of pressure losses of plate heat exchangers is conducted. The calculated Fanning friction factor is consistent with data from open literature.

(ii) Experimentally, the dependence of Fanning friction factor on distance between ports L_{port} is determined. In case of corrugation pattern HH (chevron angle $\varphi > 60^\circ$), Fanning friction factor $f_{ch}(L_{port})$ increases with increase in length L_{port}; in case of corrugation

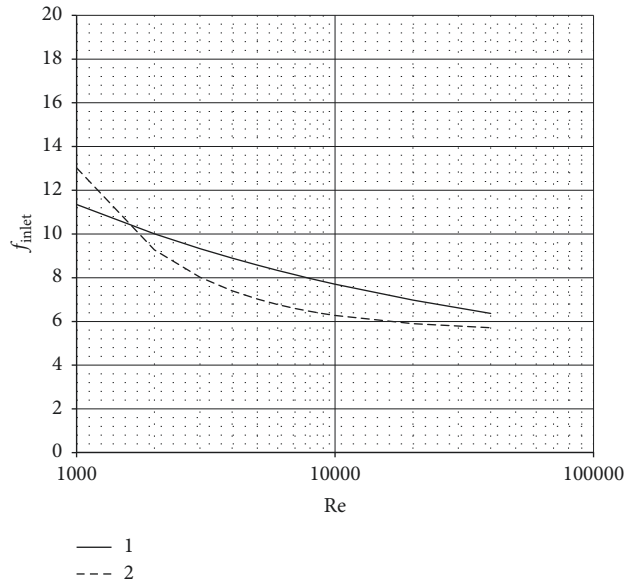

FIGURE 17: Pressure drop factor f_{inlet} for distribution zone from (i) equation (43) [23] and (ii) equation (16) the of three-component model.

pattern LL ($\varphi < 30^{\circ}$) in contrast, friction factor decreases with increase in length L_{port}. This dependence is confirmed by the data published in open literature.

(iii) For pressure losses in PHE, the enhanced three-component model is offered. This model accounts for the hydraulic resistance of distribution zones and the correlations for corrugated field. It corresponds to experimental data with an error up to 10%.

(iv) On the basis of three-component model is explained why at chevron angles $\varphi > 60^{\circ}$ Fanning friction factor $f_{ch}(L_{port})$ increases with increase in length L_{port}, and in case of $\varphi < 30^{\circ}$ in contrast, friction factor decreases with increase in length L_{port}.

(v) The portion of hydraulic resistance of distribution zone in general resistance of channel is calculated. This portion can be considerably (up to 70%) in case of corrugation angles $\varphi < 30^{\circ}$. For corrugation angles of $\varphi > 60^{\circ}$, it can reach 10–15%.

(vi) Comparison of the received dependence of hydraulic resistance of a distribution zone on the Reynolds number with the known data from literature is carried out. Good correspondence is obtained.

Nomenclature

A: Area of PHE (m^2)
B: Width (m)
D: Port diameter (m)
D_e: Equivalent diameter = $2t$ (m)
D_h: Hydraulic diameter = $2t$/FK (m)
F: Fanning friction factor, dimensionless
FK: Surface enlargement factor, dimensionless
L: Length (m)
Re: Reynolds number, $Re = \rho w_{sp} D_e/\mu$, dimensionless
t: Wave amplitude (m)
T: Temperature, °C
IR: Inlet pressure drop ratio, dimensionless
w: Velocity (m/s)
X: Relative length of corrugated field, dimensionless
Δp: Pressure losses, Pa
Δ_{wall}: Wall thickness (m)
Λ: Wavelength of corrugation (m)
λ: Heat conduction coefficient (W/mK)
μ: Dynamic viscosity (kg/(m·s))
ρ: Density (kg/m^3)
φ: Chevron corrugation angle relative to flow direction, degree
corr: Corrugation
ch: Channel
inlet: Inlet
mean: Mean
outlet: Outlet
pipe: Pipeline
pl: Plate
port: Port distance
proj: Projection
wall: At wall temperature.

Data Availability

The measurement data used to support the findings of this study have not been made available because these data are business secret of FUNKE Wärmeaustauscher Apparatebau GmbH.

Conflicts of Interest

The authors declare that there are no conflicts of interest regarding the publication of this paper.

Acknowledgments

The authors would like to thank our employer FUNKE Wärmeaustauscher Apparatebau GmbH for providing the opportunity to publish this article.

References

[1] F. Akturk, "Experimental investigation of the characteristics of a chevron type gasketed plate heat exchanger," in *Proceedings of the 6th International Advanced Technologies Symposium*, pp. 172–178, Elazig, Turkey, May 2011.

[2] R. L. Amalfi, "Two-phase heat transfer mechanisms within plate heat exchanger: experiments, modeling and simulations," Ecole Polytechn. Federale de Lausanne, Lausanne, Switzerland, These N6856, diss., 2016.

[3] R. Bögert and A. Bölcs, "Global performance of a prototype brazed plate heat exchanger in a large reynolds number range," *Experimental Heat Transfer*, vol. 8, no. 4, pp. 293–311, 1995.

[4] M. P. Bond, *Plate Heat Exchangers for Effective Heat Transfer*, Institution of Chemical Engineers, London, UK, GKD-ID: 57277, Band 162/67, 1981.

[5] A. Cooper and J. D. Usher, "Heat transfer correlations," in *Hemisphere Handbook of Heat Exchanger Design*, G. F. Hewitt, Ed., Hemisphere Publishing, Washington, DC, USA, 1983.

[6] D. Dovic and S. Svaic, "Experimental and numerical study of the flow and heat transfer in plate heat exchanger channels," in *Proceedings of the International Refrigeration and Air Conditioning Conference*, vol. R097, pp. 1–8, West Lafayette, IN, USA, July 2004.

[7] D. Dovic, B. Palm, and S. Švaić, "Generalized correlations for predicting heat transfer and pressure drop in plate heat exchanger channels of arbitrary geometry," *IJHMT*, vol. 52, no. 19-20, pp. 4553–4563, 2009.

[8] M. S. Khan and M. C. Chyu, "Evaporation in flooded corrugated plate heat exchangers with ammonia and ammonia/miscible oil," HTRI, Navasota, TX, USA, RP-1352. Final Report, 2010.

[9] W. W. Focke, J. Zachariades, and I. Olivier, "The effect of the corrugation inclination angle on the thermohydraulic performance of plate heat exchangers," *International Journal of Heat and Mass Transfer*, vol. 28, no. 8, pp. 1469–1479, 1985.

[10] I. Gherasim, M. Taws, N. Galanis, and C. T. Nguyen, "Heat transfer and fluid flow in a plate heat exchanger part I. Experimental investigation," *International Journal of Thermal Sciences*, vol. 50, no. 8, pp. 1492–1498, 2011.

[11] C. Gulenoglu, F. Akturk, S. Aradag, N. Sezer Uzol, and S. Kakac, "Experimental comparison of performances of three different plates for gasketed plate heat exchangers," *International Journal of Thermal Sciences*, vol. 75, pp. 249–256, 2014.

[12] R. L. Heavner, H. Kumar, H. Kumar, and A. S. Wanniarachchi, "Performance of an industrial plate heat exchanger: effect of chevron angle," in *Proceedings of the AIChE Symposium Series*, vol. 89, pp. 262–267, Heat Transfer-Atlanta, St. Louis, MO, USA295, , November 1993.

[13] E. Lee, H. Kang, J. Son, and Y. Kim, "The performance characteristics of plate heat exchangers used in District Heating and Cooling with geometric design parameters," in *Proceedings of the 13th International Symposium on District Heating and Cooling*, Copenhagen, Denmark, September 2012.

[14] H. Martin, "A theoretical approach to predict the performance of chevron-type plate heat exchangers," *Chemical Engineering and Processing: Process Intensification*, vol. 35, no. 4, pp. 301–310, 1996.

[15] A. Muley and R. M. Manglik, "Enhanced heat transfer characteristics of single-phase flows in a plate heat exchanger with mixed chevron plates," *Journal of Enhanced Heat Transfer*, vol. 4, no. 3, pp. 187–201, 1997.

[16] A. Muley and R. M. Manglik, "Experimental study of turbulent flow heat transfer and pressure drop in a plate heat exchanger with chevron plates," *Journal of Heat Transfer*, vol. 121, no. 1, pp. 110–117, 1999.

[17] R. K. Shah and W. W. Focke, "Plate heat exchangers and their design theory," in *Heat Transfer Equipment Design*, R. K. Shah, E. C. Subbarao, and R. A. Maskelkar, Eds., pp. 227–254, Hemisphere Publishing Corp., Waschington, DC, USA, 1988.

[18] K. Shaji and S. K. Das, "Effect of plate characteristics on axial dispersion and heat transfer in plate heat exchangers," *Journal of Enhanced Heat Transfer*, vol. 135, no. 4, article 041801, 2013.

[19] B. Thonon, R. Vidil, and C. Marvillet, "Recent research and developments in plate heat exchangers," *Journal of Enhanced Heat Transfer*, vol. 2, no. 1-2, pp. 149–155, 1995.

[20] L. Wang, B. Sundén, and R. M. Manglik, *Plate Heat Exchangers: Design, Applications and Performance*, WIT Press, Southampton, UK, 2007.

[21] J. J. Klemes, O. Arsenyeva, P. Kapustenko, and L. Tovazhnyanskyy, *Compact Heat Exchangers for Energy Transfer Intensification: Low Grade Heat and Fouling Mitigation*, CRC Press, Boca Raton, FL, USA, 2015.

[22] O. P. Arsenyeva, L. L. Tovazhnyanskyy, P. O. Kapustenko, and O. V. Demirskiy, "Heat transfer and friction factor in criss-cross flow channels of plate-and-frame heat exchangers," *Theoretical Foundations of Chemical Engineering*, vol. 46, no. 6, pp. 634–641, 2012.

[23] O. Arsenyeva, P. Kapustenko, L. Tovazhnyanskyy, and G. Khavin, "The influence of plate corrugations geometry on plate heat exchanger performance in specified process conditions," *Energy*, vol. 57, pp. 201–207, 2013.

[24] http://www.funke.de.

[25] R. J. Moffat, "Describing the uncertainties in experimental results," *Experimental Thermal and Fluid Science*, vol. 1, no. 1, pp. 3–17, 1988.